

Hierarchical mean-field approach to the J_1 - J_2 Heisenberg model on a square lattice

L. Isaev¹, G. Ortiz¹, and J. Dukelsky²

¹*Department of Physics, Indiana University, Bloomington IN 47405, USA*

²*Instituto de Estructura de la Materia - CSIC, Serrano 123, 28006 Madrid, Spain*

We study the quantum phase diagram and excitation spectrum of the frustrated J_1 - J_2 spin-1/2 Heisenberg Hamiltonian. A new hierarchical mean-field approach, at the heart of which lies the idea of identifying *relevant* degrees of freedom, is developed. Thus, by performing educated, manifestly symmetry preserving mean-field approximations, we unveil the fundamental properties of the system. We then compare various coverings of the square lattice with plaquettes, dimers and other degrees of freedom, and show that only the *symmetric plaquette* covering, which reproduces the original Bravais lattice, leads to the correct phase diagram. The intermediate quantum paramagnetic phase is shown to be a (singlet) *plaquette crystal*, whose lattice symmetry group is compatible with that of the neighbouring Néel phase connected by a continuous Landau transition. We also introduce fluctuations around the hierarchical mean-field solutions, and demonstrate that in the paramagnetic phase the ground and first excited states are separated by a finite gap, which closes in the Néel and columnar phases. We conclude that quantum phase transitions can be properly described within the Ginzburg-Landau-Wilson paradigm, therefore, ruling out the deconfined quantum criticality scenario for this model.

PACS numbers: 05.30.-d, 75.10.Jm, 64.70.Tg

I. INTRODUCTION

One of the primary goals of modern condensed matter physics is the characterization of strongly correlated quantum systems. A large class of such materials is represented by frustrated antiferromagnets, which are believed to exhibit a variety of novel states of matter at sufficiently strong coupling. Growing experimental evidence indicates that layered materials such as $\text{Li}_2\text{VO}(\text{Si}, \text{Ge})\text{O}_4$ ³, VOMoO_4 ⁴ and $\text{BaCdVO}(\text{PO}_4)_2$ ⁵ can be adequately described by an antiferromagnetic Heisenberg model with frustrating next- and next-next-nearest neighbor interactions. As a result, the study of low-dimensional magnets and their frustration-driven quantum phase transitions have attracted a lot of theoretical attention in the last decade^{1,2}.

A canonical model, used for the investigation of this kind of physical phenomena, is the spin-1/2 Heisenberg model on a square lattice with competing nearest (J_1) and next-nearest (J_2) neighbor antiferromagnetic interactions (J_1 - J_2 model). Despite numerous analytical and numerical efforts, its phase diagram continues to stir certain controversy (for a review of recent achievements, see Ref. 2). While existence of the Néel-ordered phase at small frustration ratio J_2/J_1 , and of the columnar antiferromagnetic state at large J_2/J_1 is widely established, properties of the intermediate quantum paramagnetic phase, which occurs around the maximum frustration point $J_2/J_1 = 1/2$ are still under debate. Various methods have been recently applied to characterize this phase, such as Green's function Monte Carlo^{6,7,8}, coupled cluster methods⁹, series expansions¹⁰ and field-theoretical methods^{11,12,13}. As a result, several possible scenarios were proposed in this intermediate region, namely: spin liquid⁷, preserving translational and rotational symmetries of the lattice, as well as various lattice

symmetry breaking phases, out of which the dimer^{12,14}, and the *plaquette resonating valence bond* phases⁶ are worth mentioning.

Not surprisingly, the nature itself of the quantum phase transition separating the Néel-ordered and quantum paramagnetic phases is also under scrutiny. The most dramatic, and at the same time original, scenario¹⁵ is believed to violate the Ginzburg-Landau-Wilson paradigm of phase transitions¹⁶ which revolves around the concept of an order parameter. Such point of view is based on the observation that there are different spontaneously broken symmetries in the Néel and quantum paramagnetic phases, which thus cannot be connected by a group-subgroup relation. The former, of course, breaks the $SU(2)$ invariance of the Hamiltonian and lattice translational symmetry T ^{17,18}, but preserves the four-fold rotational symmetry of the square C_4 . On the other hand, the paramagnetic phase is known to restore the spin-rotational symmetry and is believed to break T and C_4 , due to spontaneous formation of dimers along the links of the lattice^{12,14}. It follows then, that these two phases can not be joined by the usual Landau second-order critical point. This phase transition can either be of the first-order¹⁹ (the latest coupled cluster calculations⁹, however, seem to rule out this possibility), or represent an example of a second order critical point¹⁵, which cannot be described in terms of a bulk order parameter, but rather in terms of emergent fractional excitations (spinons), which become deconfined right at the critical point.

However, numerical evidence concerning the structure of the non-magnetic phase is quite controversial. Indeed, the results of spin-wave calculations¹², large- N expansions¹⁴, and calculations using the density matrix renormalization group combined with Monte-Carlo simulations⁸ are believed to indicate the emergence of a dimer order. On the other hand, Monte-Carlo⁶ and cou-

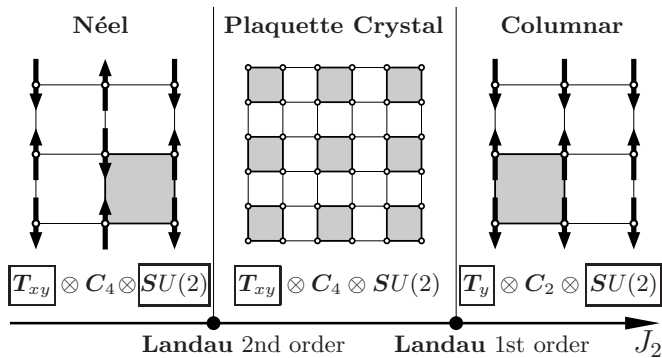


FIG. 1: A schematic phase diagram of the J_1 - J_2 model, summarizing our results. J_2 (in units of J_1) starts at 0 on the left and increases towards the right side of the axis. In each phase we show spontaneously broken (framed symbols) and unbroken symmetries (usual symbols). The translational invariance is broken along both directions in the Néel and paramagnetic phases, and only along the y -direction in the columnar phase. This fact is indicated by the subscripts xy and y after T .

pled cluster calculations⁹, and analytical results¹¹ seem to support the presence of C_4 symmetry in the paramagnetic phase. In the absence of a reliable numerical or analytical proof of the existence of a dimer order in the non-magnetic region, there is no apparent reason to believe in the deconfined quantum criticality scenario. Although there apparently exists numerical evidence²⁰, at the moment of writing the authors are unaware of a local Hamiltonian in space dimensions larger than one, rigorously proven to exhibit the type of quantum critical point discussed in Ref. 15. Interestingly, it was demonstrated in Ref. 21 that a two-dimensional (2D) lattice model can possess a *first order* quantum critical point, which exhibits deconfined excitations.

All in all, the complexity of the methods used to infer properties of the paramagnetic phase and the variety of different conclusions have created a certain degree of confusion. Our goal in the present paper is to try to clarify some of this controversy by proposing a controlled and manifestly symmetry preserving method, geared to computing ground state properties of the J_1 - J_2 model. Our approach is based on the recently proposed systematic methodology to investigate the behavior of strongly coupled systems²², whose main idea consists of identifying *relevant* degrees of freedom and performing an educated approximation, called the hierarchical mean-field (HMF), to uncover the phase diagram and other properties of the system of interest. In a future work these ideas will be coupled to a new, variational with respect to the energy, renormalization group approach which thus adapts to the concept of relevant degrees of freedom.

In the present work we construct HMF approximations for the J_1 - J_2 model. The crux of our method is the identification of a *plaquette* (spin cluster 2×2 or even larger 4×4 (*superplaquette*) symmetry-preserving cluster) as the relevant elementary degree of freedom,

which captures necessary quantum correlations to represent essential features of the phase diagram. The importance of this degree of freedom was realized only recently in the present context¹¹, and somewhat earlier in connection with $SU(4)$ spin-orbital²³ and Hubbard²⁴ models. Besides being variational, our formalism has the attractive feature of preserving fundamental lattice and $SU(2)$ symmetries of the Hamiltonian, by utilizing the Schwinger boson-type representation and the Racah algebra technology. Remarkably, such simple mean-field calculation already yields all known results, concerning the phase diagram of the J_1 - J_2 model, with a good accuracy, namely: existence of a Néel-ordered phase with antiferromagnetic wavevector (π, π) and spin-wave type excitations for $J_2/J_1 \lesssim 0.42$, a non-magnetic intermediate gapped phase, separated by a second order quantum phase transition, and a first order transition point, which is characterized by the discontinuous disappearance of the energy gap and connects the paramagnetic state with the columnar antiferromagnetic phase at $(\pi, 0)$ and $(0, \pi)$ for $J_2/J_1 \gtrsim 0.66$.

We emphasize that our investigation primarily focuses on a symmetry analysis of the various phases. Out of the many possible coarse graining scenarios, such as covering of the 2D lattice with plaquettes, dimers and crosses, only the C_4 -*symmetry preserving* plaquette (or superplaquette) covering (which reproduces the original Bravais lattice) displays the correct phase diagram. For all other scenarios, including dimerized (bond-ordered) phases, we were unable to reproduce all known quantum phase transition points of the model. Our results are fully consistent with the Landau theory of phase transitions. In fact, the requirement of its validity unambiguously fixes the spatial symmetry of the paramagnetic phase to be C_4 and rules out any dimerized phases. Indeed, we found that a *plaquette crystal* phase, which preserves spin and lattice rotational symmetries, is realized in this region.

Next two sections are devoted to the formulation of the HMF approximation. Then, we present results of our calculations and close the paper with a discussion. A main result of the paper is summarized in Fig. 1, which emphasizes symmetry relations between different phases of the model.

II. THE PLAQUETTE DEGREE OF FREEDOM

We consider the spin-1/2 antiferromagnetic Heisenberg model with frustrated next-nearest neighbor interactions J_2 , defined on a 2D bipartite lattice with N sites:

$$H = J_1 \sum_{\langle i,j \rangle} \mathbf{S}_i \cdot \mathbf{S}_j + J_2 \sum_{\langle\langle i,j \rangle\rangle} \mathbf{S}_i \cdot \mathbf{S}_j. \quad (1)$$

As mentioned already in the Introduction, we choose the plaquette, Fig. 2, as our *elementary* degree of freedom. Then, assuming that N is chosen appropriately, the entire lattice can be covered with such plaquettes in a sub-exponentially²³ ($\sim 2^{\sqrt{N}}$) large number of ways.

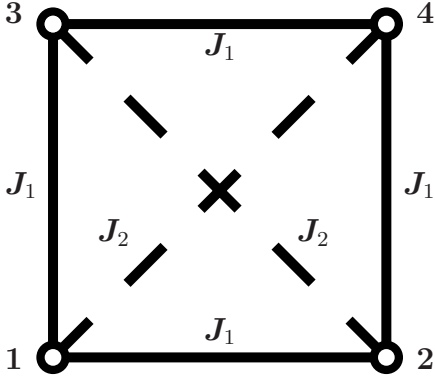


FIG. 2: A single 2×2 plaquette has each vertex occupied by a $S = 1/2$ spin. The diagonal spins interact through a Heisenberg term of strength J_2 , while nearest neighbor spins interact with strength J_1 .

Aiming at illustrating the main idea of the method, in this section we consider in detail only the symmetric covering of the lattice with 2×2 plaquettes, which preserves the C_4 lattice symmetry, see Fig. 3, although later the displaced covering (Fig. 4), which breaks C_4 down to C_2 (two-fold symmetry axis), and the case of larger plaquettes (superplaquettes) will be analyzed as well.

It is convenient to take as a basis the states

$$|a\rangle = |l_1 l_2 L M\rangle, \quad (2)$$

where $\mathbf{l}_1 = \mathbf{S}_1 + \mathbf{S}_4$ and $\mathbf{l}_2 = \mathbf{S}_2 + \mathbf{S}_3$ are total spins of the plaquette diagonals, while $\mathbf{L} = \mathbf{l}_1 + \mathbf{l}_2$ is the total spin of the entire plaquette and M is its z -component. In this basis the Hamiltonian of a single plaquette,

$$H_{\square} = J_1(\mathbf{S}_1 + \mathbf{S}_4)(\mathbf{S}_2 + \mathbf{S}_3) + J_2(\mathbf{S}_1 \cdot \mathbf{S}_4 + \mathbf{S}_2 \cdot \mathbf{S}_3) \quad (3)$$

is diagonal with eigenvalues

$$\begin{aligned} \epsilon_{l_1 l_2 L} = & \frac{J_1}{2} [L(L+1) - l_1(l_1+1) - l_2(l_2+1)] + \\ & + \frac{J_2}{2} [l_1(l_1+1) + l_2(l_2+1) - 3]. \end{aligned} \quad (4)$$

We note that the basis of Eq. (2) is a natural one and allows us to explicitly label states with corresponding representations of $SU(2)$.

The next step is to establish how a plaquette couples to the rest of the system. In Fig. 3 we show the symmetric plaquette covering of the 2D lattice. In the figure the vertices of every non-central plaquette are similarly labeled by the numbers 5, 6, 7, 8, and total spins of diagonals are $\mathbf{l}_3 = \mathbf{S}_5 + \mathbf{S}_8$ and $\mathbf{l}_4 = \mathbf{S}_6 + \mathbf{S}_7$. In the uncoupled basis the matrix elements of inter-plaquette interaction are:

$$\begin{aligned} (H_{\text{int}}^{\sigma})_{a_1 a_2}^{a'_1 a'_2} = & \sum_{LM} \langle \lambda'_1 \lambda'_2, LM | H_{\text{int}}^{\sigma} | \lambda_1 \lambda_2, LM \rangle \times \\ & \times \langle L'_1 M'_1 L'_2 M'_2 | L'_1 L'_2 LM \rangle \langle L_1 M_1 L_2 M_2 | L_1 L_2 LM \rangle, \end{aligned} \quad (5)$$

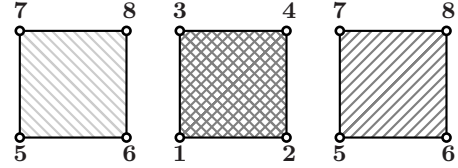
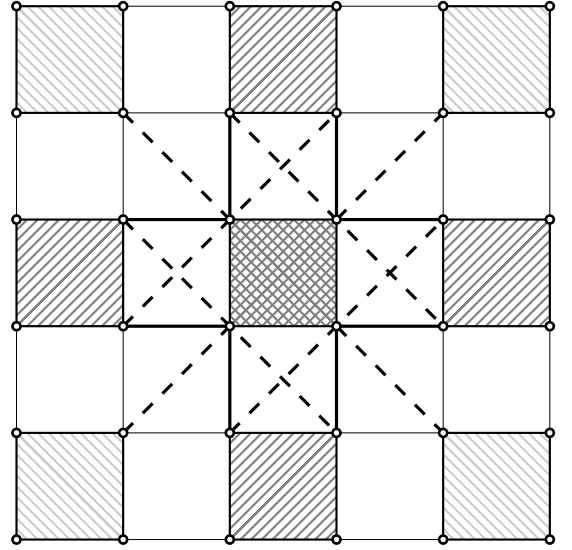


FIG. 3: Symmetric covering of the 2D lattice with 2×2 plaquettes. Each plaquette is connected to 4 nearest and 4 next-nearest neighbors.

where $\sigma = 1$ ($\sigma = 2$) corresponds to the nearest (next-nearest) neighbor interaction and $\mathbf{L} = \mathbf{L}_1 + \mathbf{L}_2$. In this equation we introduced the notations $\lambda_1 = \{l_1 l_2 L_1\}$, $\lambda_2 = \{l_3 l_4 L_2\}$, and similarly for the primed indices. Because each plaquette has 4 nearest neighbors and 4 next-nearest neighbors (see Fig. 3), the symmetrized next-nearest neighbor interaction is:

$$\begin{aligned} \langle \lambda'_1 \lambda'_2, LM | H_{\text{int}}^2 | \lambda_1 \lambda_2, LM \rangle = & J_2 \rho_{L_1 L_2}^{L'_1 L'_2}(L) \times \\ & \times \left(S_3^{\lambda'_1 \lambda_1} S_6^{\lambda'_2 \lambda_2} + S_1^{\lambda'_1 \lambda_1} S_8^{\lambda'_2 \lambda_2} + S_2^{\lambda'_1 \lambda_1} S_7^{\lambda'_2 \lambda_2} + S_4^{\lambda'_1 \lambda_1} S_5^{\lambda'_2 \lambda_2} \right). \end{aligned} \quad (6)$$

while the symmetrized nearest neighbor plaquette interaction has the form:

$$\begin{aligned} \langle \lambda'_1 \lambda'_2, LM | H_{\text{int}}^1 | \lambda_1 \lambda_2, LM \rangle = & J_1 \rho_{L_1 L_2}^{L'_1 L'_2}(L) \times \\ & \times [(S_1^{\lambda'_1 \lambda_1} + S_4^{\lambda'_1 \lambda_1}) (S_6^{\lambda'_2 \lambda_2} + S_7^{\lambda'_2 \lambda_2}) + \\ & + (S_2^{\lambda'_1 \lambda_1} + S_3^{\lambda'_1 \lambda_1}) (S_5^{\lambda'_2 \lambda_2} + S_8^{\lambda'_2 \lambda_2})] + \\ & + 2 \langle \lambda'_1 \lambda'_2, LM | H_{\text{int}}^2 | \lambda_1 \lambda_2, LM \rangle, \end{aligned} \quad (7)$$

In Eqs. (6) and (7) the symbols $S_n^{\lambda' \lambda} = \langle \lambda' || S_n || \lambda \rangle$ denote reduced matrix elements of the n -th spin operator, and:

$$\rho_{L_1 L_2}^{L'_1 L'_2}(L) = \frac{1}{4} (-1)^{L+L'+L_1} \begin{Bmatrix} L'_1 & L'_2 & L \\ L_2 & L_1 & 1 \end{Bmatrix},$$

where $\{\dots\}$ are Wigner $6j$ symbols (or Racah coefficients)²⁵.

Let us now identify the plaquette degree of freedom with a Schwinger boson which creates a specific state of the plaquette. The Hamiltonian Eq. (1) in the plaquette basis can then be expressed as:

$$H = \sum_{i,a} \epsilon_a \gamma_{ia}^\dagger \gamma_{ia} + \sum_{\langle ij \rangle} (H_{\text{int}}^1)_{a_1 a_2}^{a'_1 a'_2} \gamma_{ia'_1}^\dagger \gamma_{ja'_2}^\dagger \gamma_{ia_1} \gamma_{ja_2} + \sum_{\langle\langle ij \rangle\rangle} (H_{\text{int}}^2)_{a_1 a_2}^{a'_1 a'_2} \gamma_{ia'_1}^\dagger \gamma_{ja'_2}^\dagger \gamma_{ia_1} \gamma_{ja_2}, \quad (8)$$

where the operator γ_{ia}^\dagger creates a boson on site i of the *plaquette* lattice (which contains $N_\square = N/4$ sites) in the state, denoted by an index a , running through the entire single-plaquette Hilbert space (of dimension $2^4 = 16$) and the summation is performed over doubly repeated dummy indices. The unphysical states are eliminated by enforcing the local constraint $\sum_a \gamma_{ia}^\dagger \gamma_{ia} = 1$. In what follows, we impose periodic boundary conditions on the plaquette lattice.

The bosonic operators γ_{ia} define the hierarchical language²² for our problem. It will be used in the next section, where we develop an approximation scheme for diagonalizing the Hamiltonian of Eq. (8).

III. HIERARCHICAL MEAN-FIELD APPROXIMATION

As it follows from Eq. (4), the lowest single-plaquette state has the energy $\epsilon_{1100}/4 = -J_1/2 + J_2/8$ per spin, which, when $J_2 = 0$, gives only the energy of a classical 2D antiferromagnet. Thus, it is necessary to take into account the interaction term in Eq. (8).

The HMF approximation is a mean-field approach, performed on the relevant degrees of freedom. In the present section we discuss only the simplest one – a Hartree-Fock like (HF) approximation. A possible way to include fluctuation corrections is presented in Appendix B. The HF approximation introduces the mixing of single-plaquette states which minimizes the total energy of the system and is based on a canonical transformation among the bosons, which we will restrict to be uniform (plaquette independent):

$$\gamma_{ia} = R_a^n \Gamma_{in}. \quad (9)$$

The real matrix R satisfies canonical orthogonality and completeness relations:

$$R_a^n R_a^{n'} = \delta_{nn'}; \quad R_a^n R_{a'}^n = \delta_{aa'}$$

A *translationally invariant* variational ansatz for the ground state (vacuum) is a boson condensate in the lowest HF single-particle energy state ($n = 0$):

$$|\text{HF}\rangle = \prod_i \Gamma_{i0}^\dagger |0\rangle, \quad (10)$$

and since it has one boson per plaquette, there is no need to impose the Schwinger boson constraint in the calculation.

Minimizing the total energy with respect to R , we arrive at the self-consistent equation:

$$\left\{ \epsilon_a \delta_{aa'} + \sum_\sigma z_\sigma (H_{\text{int}}^\sigma)_{a'a_2}^{aa_1} R_{a_1}^0 R_{a_2}^0 \right\} R_{a'}^n = \epsilon_n R_a^n, \quad (11)$$

where $z_1 = z_2 = 4$ are the nearest- and next-nearest coordination numbers. The ground state energy (GSE) per spin is then given by the expression:

$$\frac{E_0}{N} = \frac{\langle \text{HF} | H | \text{HF} \rangle}{N} = \frac{1}{8} \left(\epsilon_0 + \sum_a \epsilon_a (R_a^0)^2 \right), \quad (12)$$

with ϵ_0 being the lowest eigenvalue of Eq. (11).

Another fundamental quantity to compute is the polarization of spins within a plaquette:

$$\langle \text{HF} | S_{in}^z | \text{HF} \rangle = (S_n^z)_{a'a} R_{a'}^0 R_a^0,$$

where $n = 1, \dots, 4$ is the spin index, and the matrix elements (determined from the Wigner-Eckart theorem) are:

$$(S_n^z)_{a'a} = \langle l'_1 l'_2 L' M' | S_n^z | l_1 l_2 L M \rangle = (-1)^{L+L'+1} \delta_{MM'} \frac{\langle 10 L M | 1 L L' M \rangle}{\sqrt{2L'+1}} \langle l'_1 l'_2 L' || S_n || l_1 l_2 L \rangle. \quad (13)$$

This enables us to define the staggered and collinear (along x and y axes) magnetizations:

$$\begin{aligned} M_{\text{stag}} &= (1/4) \langle \text{HF} | S_1^z + S_4^z - S_2^z - S_3^z | \text{HF} \rangle; \\ M_{\text{col}}(x) &= (1/4) \langle \text{HF} | S_1^z + S_2^z - S_3^z - S_4^z | \text{HF} \rangle; \\ M_{\text{col}}(y) &= (1/4) \langle \text{HF} | S_1^z + S_3^z - S_2^z - S_4^z | \text{HF} \rangle. \end{aligned} \quad (14)$$

Notice the extreme simplicity of the HMF approximation. The reason why it is able to realize meaningful results is that the plaquette degree of freedom seems to contain the main correlations defining the physics behind the Hamiltonian of Eqs. (1), and (8). To avoid confusion, we emphasize that the HF approximation and the fluctuation theory of Appendix B are physically (and obviously mathematically) different from the spin-wave or canonical Schwinger-Wigner boson mean-field approach to spin systems²⁶. In particular, we make no assumption about the underlying ground state, thus allowing for an interplay of various quantum phases. Moreover, it will be demonstrated, that the collective excitation spectra in each phase consistently reflect spontaneously broken symmetries, unlike the usual Schwinger boson case²⁶, in which one obtains gapped excitations.

IV. GROUND STATE PROPERTIES OF THE MODEL

Our choice of the plaquette as an elementary degree of freedom remains unjustified at this point. In order to

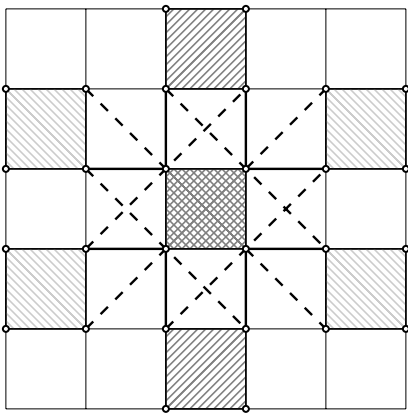


FIG. 4: The displaced plaquette covering. Notice that the C_4 symmetry is broken down to C_2 .

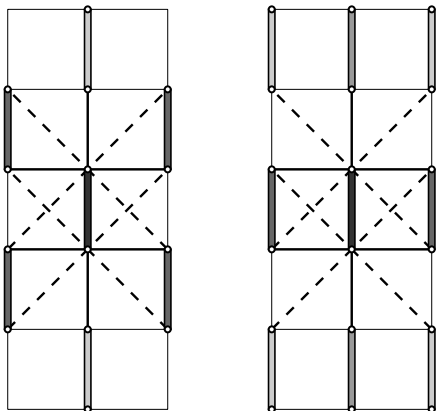


FIG. 5: Connectivity of the dimer lattice for symmetric (right panel) and displaced dimer coverings (left panel). The rotational C_4 symmetry is lowered to C_2 in both cases.

show its relevance we extended the analysis of the previous two sections to several other coarse grainings (besides the symmetric plaquette covering, case (a), shown in Fig. 3): (b) *superplaquette* (spin cluster 4×4) degree of freedom, covering the lattice in such a way that C_4 is preserved (see Appendix A for details); (c) displaced plaquette covering of the lattice, Fig. 4; (d) symmetric and displaced *dimer* coverings, shown respectively in right and left panels of Fig. 5; (e) *cross* degree of freedom, Fig. 6. One should observe that symmetries of the original Bravais lattice are preserved only in cases (a) and (b). In cases (c) and (d) the lattice rotational symmetry C_4 is lowered to C_2 . Case (e) is special in the sense that an isolated degree of freedom does not possess a singlet ground state. For each of the above cases we iteratively solve Eq. (11) and compute the GSE (12), and staggered and collinear magnetizations (14). The main message, which we would like to convey in this section is that only the plaquette degree of freedom (of any size) is relevant for constructing the phase diagram of the Hamiltonian of

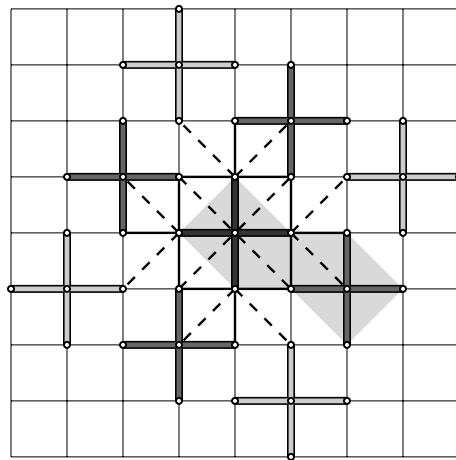


FIG. 6: Covering of the lattice with crosses – arrays of five spins. Since one cross cannot form a singlet, it is necessary to double the unit cell, as indicated by the gray shading. This choice of a degree of freedom clearly preserves the C_4 symmetry, but the resulting lattice breaks it.

Eq. (1).

Let us focus first on cases (a) and (b). The resulting GSE as a function of J_2/J_1 is shown in Fig. 7. One immediately observes a level-crossing at $J_2^{c1} \approx 0.67J_1$, indicating the first-order transition and a second-order quantum critical point at $J_2^{c2} \approx 0.42J_1$, which is supported by a jump of the second order derivative d^2E_0/dJ_2^2 , Fig. 8. Both Néel and columnar phases are characterized by spontaneously broken $SU(2)$ symmetry. The former exhibits a nonvanishing staggered magnetization, M_{stag} , while the latter has nonzero collinear magnetization along the x -direction, $M_{\text{col}}(x)$. Both order parameters disappear in the paramagnetic phase, suggesting that $SU(2)$ is restored. These results are summarized in Fig. 9, from which it also follows that the phase transition at J_2^{c1} is continuous, while J_2^{c2} corresponds to a first-order transition point. We remind, in this connection, that our approach does not explicitly break the spin rotational symmetry, thus allowing for the treatment of competing ground states. As it was expected, considering a larger elementary degree of freedom – superplaquette – leads to a significant improvement of the GSE and reduction of the magnetization, due to larger quantum fluctuations. The qualitative finite-size scaling, using these two sizes (2×2 and 4×4), indicates that $E_0(J_2 = 0)/N \rightarrow -0.64J_1$ and $M_z(J_2 = 0) \rightarrow 0.39$ in the thermodynamic limit, a satisfying result for a HF approximation, which completely ignores fluctuations.

Next, we discuss in more detail the symmetry properties of the various phases in Figs. 7, 9. At all values of $J_2 \leq J_2^{c2}$, the lattice translational symmetry T is broken¹⁸, but the rotational C_4 symmetry is preserved. For $J_2 \leq J_2^{c1}$ this corresponds to a Néel-type long-range order with magnetic doubling of the unit cell and spontaneously broken $SU(2)$. At large values $J_2 \geq J_2^{c2}$, we ob-

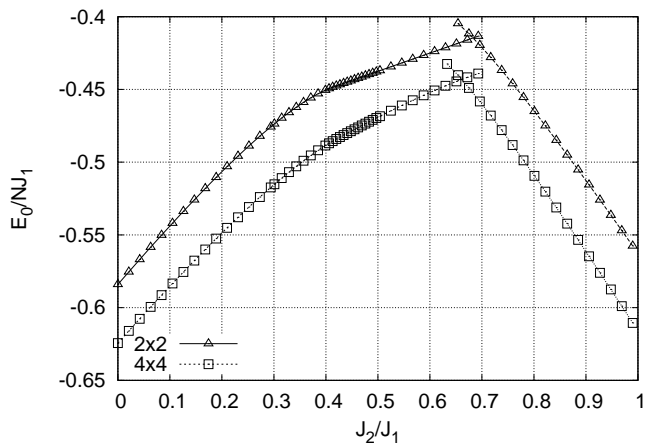


FIG. 7: Ground state energy per spin computed at the HF level for the 2×2 and 4×4 plaquette elementary degrees of freedom.

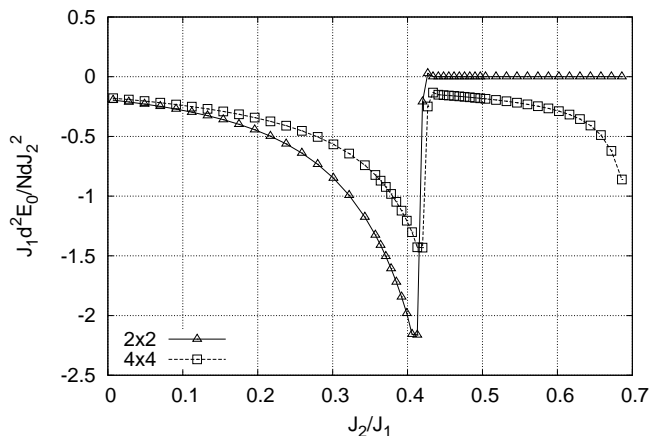


FIG. 8: Second order derivative $d^2 E_0/dJ_2^2$ for the 2×2 and 4×4 plaquette degrees of freedom. The discontinuity at $J_2/J_1 \approx 0.42$ is indicative of a second-order quantum phase transition.

serve the columnar ordering, which spontaneously breaks C_4 down to C_2 , and $SU(2)$, but partially (i.e., along one direction) restores the lattice translational symmetry. In the intermediate region $J_2 \in (J_2^{c1}, J_2^{c2})$ the spin $SU(2)$ rotational symmetry is restored. In this paramagnetic phase the ground state wavefunction is a tensor product of individual plaquette ground states (with quantum numbers $l_1 = l_2 = 1, L = M = 0$):

$$|1100\rangle = \frac{1}{\sqrt{3}} \left[2(|\uparrow_1\uparrow_4\downarrow_2\downarrow_3\rangle + |\downarrow_1\downarrow_4\uparrow_2\uparrow_3\rangle) - (|\uparrow_1\downarrow_4\uparrow_2\downarrow_3\rangle + |\uparrow_1\downarrow_4\downarrow_2\uparrow_3\rangle + |\downarrow_1\uparrow_4\uparrow_2\downarrow_3\rangle + |\downarrow_1\uparrow_4\downarrow_2\uparrow_3\rangle) \right]. \quad (15)$$

This ground state necessarily breaks the lattice translational symmetry, but preserves C_4 . In fact, the paramagnetic region on the phase diagram of Figs. 7 and 9 is

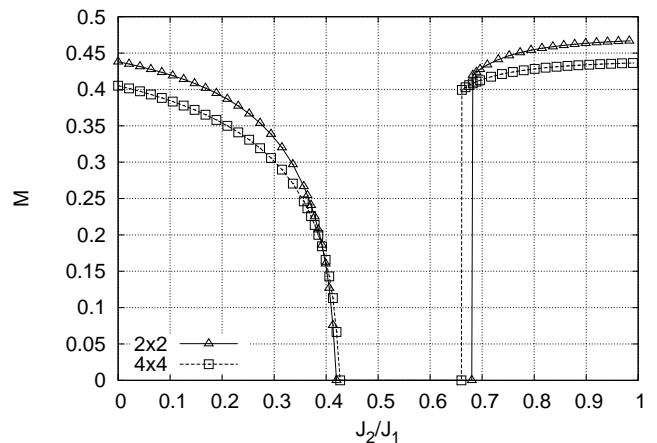


FIG. 9: Staggered magnetization, M_{stag} , for $J_2 \leq J_2^{c1}$ and collinear magnetization along the x -direction, $M_{\text{col}}(x)$, for $J_2 \geq J_2^{c2}$ for the 2×2 and 4×4 plaquette degrees of freedom, computed at the HF level. Notice the continuous phase transition at $J_2/J_1 \approx 0.42$ and a first order transition at $J_2/J_1 \approx 0.68$ (2×2) and $J_2/J_1 \approx 0.66$ (4×4).

a trivial plaquette crystal: a set of *non-interacting* plaquettes, because the expectation value of the plaquette interaction (see Eq. (8)) in the singlet state $\prod_i \gamma_{i,1100}^\dagger |0\rangle$ vanishes. An analogous situation is realized when the superplaquette is chosen as an elementary degree of freedom: the paramagnetic phase is a crystal of superplaquettes. This symmetry analysis, clearly explains the character of the two critical points. It is interesting to note that in Ref. 6 a “plaquette RVB state” has been proposed. However, later⁷ the intermediate phase was argued to be a spin liquid, i.e., a state that preserves the lattice translational symmetry.

Another way to learn about spatial symmetries in the quantum paramagnetic region is to compare magnitudes of the several lattice symmetry-breaking observables proposed in the literature. We consider the following three, introduced in Ref. 9 (in the notation of that paper):

$$F_1 = \frac{1}{N} \sum_{x,y} (-1)^x \mathbf{S}_{x,y} \mathbf{S}_{x+1,y};$$

$$F_2 = \frac{1}{N} \sum_{x,y} \mathbf{S}_{x,y} (\mathbf{S}_{x+1,y} - \mathbf{S}_{x,y+1});$$

$$F_4 = \frac{1}{N} \sum_{x,y} \mathbf{S}_{x,y} [(-1)^x \mathbf{S}_{x+1,y} + (-1)^y \mathbf{S}_{x,y+1}],$$

where indices x, y specify a spin in the 2D lattice. The operator F_4 probes the plaquette ordering, which preserves the lattice rotational symmetry, while F_1 and F_2 correspond to the columnar ordering. We note, however, that both F_1 and F_4 are already non-zero for an isolated plaquette. Here we compute the functions $F_{1,2,4}$ for case (a). Their behavior in case (b) is expected to be similar. In the plaquette representation the above operators are

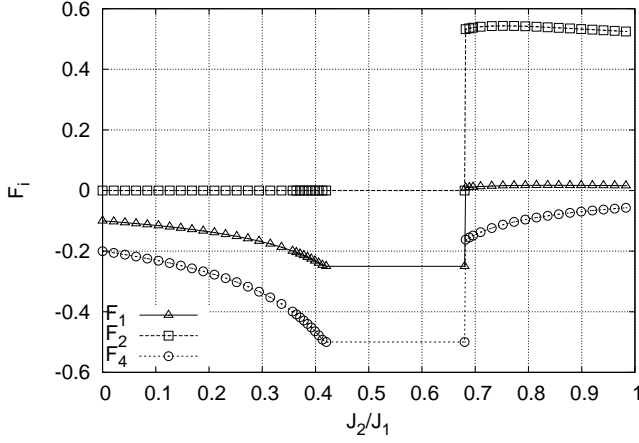


FIG. 10: HF ground state expectation values of the symmetry-breaking perturbations, given by Eq. (16), plotted as functions of J_2/J_1 for the 2×2 plaquette degree of freedom. Due to the unbroken C_4 symmetry in the Néel and paramagnetic phases, values of F_4 are twice larger than the corresponding values of F_1 , except in the columnar phase, where C_4 is spontaneously broken down to C_2 .

written as:

$$\begin{aligned}
 F_1 &= \frac{1}{N} \sum_{i,j} [(\mathcal{S}_{1;i,j} \mathcal{S}_{2;i,j} + \mathcal{S}_{3;i,j} \mathcal{S}_{4;i,j}) - \\
 &\quad - (\mathcal{S}_{2;i,j} \mathcal{S}_{5;i+1,j} + \mathcal{S}_{4;i,j} \mathcal{S}_{7;i+1,j})]; \\
 F_{2,4} &= \frac{1}{N} \sum_{i,j} [(\mathcal{S}_{1;i,j} \mp \mathcal{S}_{4;i,j})(\mathcal{S}_{2;i,j} \mp \mathcal{S}_{3;i,j}) \pm \\
 &\quad \pm (\mathcal{S}_{2;i,j} \mathcal{S}_{5;i+1,j} + \mathcal{S}_{4;i,j} \mathcal{S}_{7;i+1,j} \mp \\
 &\quad \mp \mathcal{S}_{3;i,j} \mathcal{S}_{5;i,j+1} \mp \mathcal{S}_{4;i,j} \mathcal{S}_{6;i,j+1})].
 \end{aligned} \quad (16)$$

In this equation the indices i, j are coordinates of a plaquette in the lattice.

Expectation values of the functions Eq. (16) in the HF ground state are shown in Fig. 10. Both phase transition points J_2^{c1} and J_2^{c2} are clearly seen from this plot. All functions change continuously across the second-order critical point J_2^{c1} and jump at the first-order transition point J_2^{c2} . Except in the columnar phase the values of F_4 are everywhere exactly twice larger than those of F_1 , which is an indication of the unbroken four-fold rotational symmetry of the lattice in these regions. In the columnar phase, on the other hand, this symmetry is broken and the above relation does not hold. While in the Néel and columnar phases nonlocal terms in Eq. (16) are important, in the paramagnetic state the only contribution to either expectation value comes from isolated plaquettes (local terms in Eq. (16)). This observation is consistent with properties of the ground state in the non-magnetic phase, discussed earlier in this section.

Until now we have considered only ground-state properties of the model Eq. (1). However, low-lying excited states are also of considerable interest. In particular, the paramagnetic phase is known to have gapped excita-

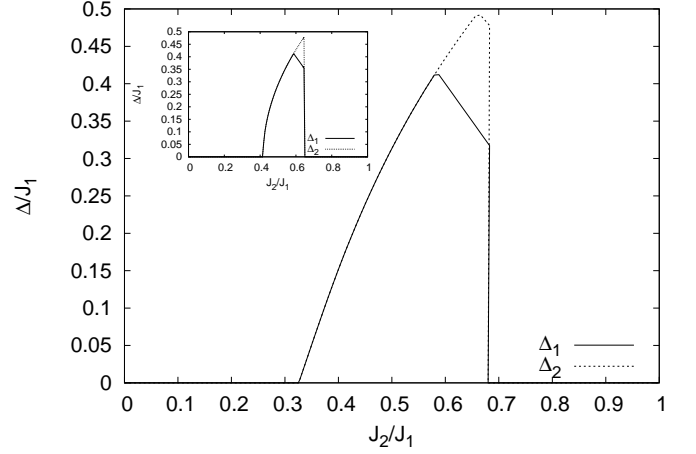


FIG. 11: The two lowest excitation energies taken at the center of the plaquette Brillouin zone. The main panel shows the self-consistent solution to Bogoliubov's equations, while the inset corresponds to the time-dependent Gross-Pitaevskii equation. The cusps in the non-magnetic phase are due to level crossing of higher excited states.

tions, while Néel and columnar phases exhibit Goldstone modes. Thus, the phase transition points J_2^{c1} and J_2^{c2} must be accompanied by the opening of a gap in the excitation spectrum: the former in a continuous and the latter in a discontinuous fashion.

In Appendix B we present a particular method to obtain the collective spectrum of the system. The main idea of this approximation is borrowed from the Bogoliubov-Fetter theory of superfluidity³⁴. Namely, assume that on each plaquette the majority of Schwinger bosons form a condensate in an appropriately chosen lowest energy state and neglect fluctuations in the number of condensed particles. We note, however, that due to the Schwinger boson constraint, this quantity has the meaning of a probability to find a given plaquette in the lowest energy HF state, rather than the number of particles. Nevertheless, we will call it the condensate fraction n_0 , which, in principle, should be determined self-consistently, and is a measure of the applicability of the entire approximation: it should satisfy the inequality $|n_0 - 1| \ll 1$. Once the condensation part is separated from γ_{ia} , what remains describes fluctuation corrections to the HF ground state. These fluctuations have rather strong effects near the phase transition points, leading to the modification of J_2^{c1} to a λ -point and its considerable shift. The value of J_2^{c2} also changes, but much less significantly. These facts imply that our approximation breaks down near the phase transition points. Indeed, in Appendix B it is shown that close to the transition, the condensate is strongly suppressed. However, deep in each phase $n_0 \sim 0.9$, thus allowing us to draw conclusions about general properties of the collective spectrum.

A complete summary of the results is given in Appendix B, here we only present the most interesting one:

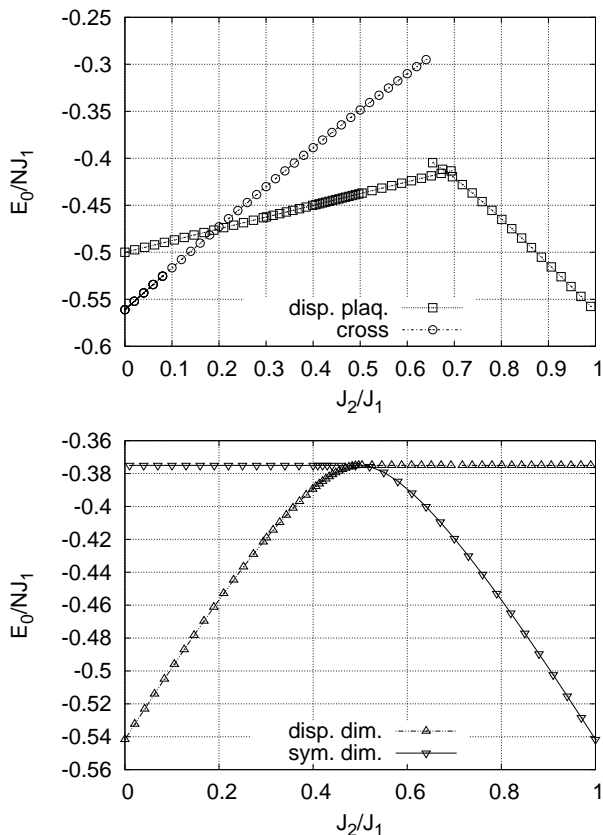


FIG. 12: HF ground state energy per spin for the displaced plaquette and cross (upper panel), and dimer (lower panel) coverings.

The gap in the excitation spectrum as a function of J_2/J_1 . Although we focus only on case (a) (2×2 plaquette), the superplaquette degree of freedom can be considered in a similar manner. The gap always occurs in momentum space at $\mathbf{k} = 0$, which reflects translational invariance of the *plaquette* lattice. Below we focus only on this point in the plaquette Brillouin zone. In fact, there are $16 - 1 = 15$ collective branches and only some of them become gapless in the phases with spontaneously broken $SU(2)$. However, in the paramagnetic phase all branches develop a gap. In Fig. 11 we show the energy gap $\Delta(J_2) = \omega(\mathbf{k} = 0, J_2)$ for the two lowest excitation branches in a system of 100×100 plaquettes, which approximates well the thermodynamic limit. The main panel shows results of the self-consistent solution to Bogoliubov's equations, which should be compared with the solution of the time-dependent Gross-Pitaevskii equation (25), shown in the inset. In the Néel and columnar phases there are two spin wave-type Goldstone modes, both of which acquire a gap in the paramagnetic phase, at J_2^{c1} and J_2^{c2} . However, as it follows from Fig. 11, positions of these points change from their HF values to: $J_2^{c1} \approx 0.33J_1$ and $J_2^{c2} \approx 0.65J_1$. The critical point J_2^{c1} was obtained by extrapolation of the staggered magneti-

zation curve (Fig. 16) to zero, while the first-order point J_2^{c2} by extrapolating the two GSE curves in Fig. 14 until intersection. The single-plaquette physical picture, discussed previously in connection with the paramagnetic phase, remains valid, e.g. the condensation occurs again in the plaquette state $|1100\rangle$. Using this observation and symmetries of the matrix elements $(H_{\text{int}}^\sigma)_{ab}^{a'b'}$, one can rigorously show the existence of a gap in the non-magnetic region. In fact, we can say, that it is a property of our HMF approximation, rather than a numerical evidence.

Finally, we comment on the results for cases (c)-(e). The corresponding GSEs are shown in Fig. 12. Contrary to the previously considered scenarios, these cases give *qualitatively* wrong phase diagrams. Indeed, if we cover the lattice with displaced plaquettes or crosses, there exists no classical spin configuration, which gives the long-range Néel order. On the other hand, such configuration exists for the columnar state. For the displaced plaquette covering the low- J_2 phase $J_2 \leq J_2^{c2}$ is an $SU(2)$ singlet, and spatially is a set of non-interacting plaquettes (notice the coincidence of 2×2 -plaquette energies in the paramagnetic phases of Figs. 7 and 12). Thus, the phase transition to the columnar state is of the first-order. For the cross covering, on the other hand, $SU(2)$ is explicitly broken for all values of J_2 , but since the columnar phase partially restores the lattice translational invariance, it is again separated from the non-magnetic state by a first-order phase transition point. The two dimer configurations, case (d), are complementary to each other in the sense that one of them has only the classical Néel state and another – only columnar phase. It follows that these configurations can have only one second-order critical point at which $SU(2)$ is restored and other symmetries remain broken. As a result, one obtains the phase diagram, shown in the lower panel of Fig. 12, which is invariant under reflection in the plane $J_2 = J_2^{c1}$. These observations imply that the coarse graining prescriptions (c)-(e) are probably a bad starting point for any approximation scheme.

V. DISCUSSION

In this section we would like to put our main results in perspective by making several summarizing remarks.

First of all, from our analysis it follows that dimer (bond) order is always unfavorable in the non-magnetic phase. Notice that even when the plaquette coverings were considered such an order did not occur, although spontaneous dimerization was not explicitly prohibited. Instead, the quantum paramagnetic phase prefers to preserve the lattice rotational symmetry, which makes the phase transition separating it from the Néel phase fit perfectly well within the Ginzburg-Landau-Wilson paradigm. The data presented for the staggered magnetization, Fig. 9, and symmetry-breaking observables, Fig. 10, indicate that the symmetry group of the Néel state is a subgroup of the symmetry group in the paramag-

netic phase, as both phases break T and preserve C_4 , but the latter also preserves $SU(2)$. On the contrary, there is no such group-subgroup relation between the paramagnetic and columnar antiferromagnetic phases. Consequently, the transition between these two states is first order. These observations are summarized in Fig. 1. Indeed, as we mentioned in the Introduction, starting from the known symmetry in the Néel state and assuming validity of the Landau theory, one can unambiguously rule out dimerized structures in the paramagnetic phase, since they break lattice rotational symmetry. The bottom line is that our results do not favor the scenario of deconfined quantum criticality, advocated in Refs. 9,15. There also exists the logical possibility that the transition between the Néel and paramagnetic orders becomes first order, a result not supported by our calculations either.

Next, we observe that despite profound differences between the 2D and 1D equivalent J_1 - J_2 models, their non-magnetic phases present some similarities. The one-dimensional model is known to be quasi-exactly solvable²⁷ at the point $J_2 = 0.5J_1$ and exhibits a paramagnetic ground state with short-range correlations for J_2 above the critical value²⁸ $J_2^c \approx 0.24J_1$ (however, due to the peculiar physics in one dimension, the critical point J_2^c is an essential singularity and, therefore, not obviously accessible for the HMF approximation of the type presented here). In this non-magnetic region the ground state is doubly degenerate, corresponding to two possible coverings of a 1D lattice with dimers, in accordance with the Lieb-Schultz-Mattis theorem²⁹. Unfortunately, a finite-size scaling calculation for the gap between the lowest and first excited energy levels, based on exact diagonalization of the 2×2 and 4×4 clusters with periodic boundary conditions, do not provide a definitive answer to the question on whether the ground state of the 2D J_1 - J_2 model becomes degenerate in the region $J_2^{c1} \leq J_2 \leq J_2^{c2}$. This is indeed what one would expect on the basis of a generalization of the Lieb-Schultz-Mattis theorem to higher space dimensions (see, e.g. Ref. 30). At the HF level, it is true that different *plaquette* coverings of the lattice have the same energy (simply because each plaquette is in its singlet ground state). However, the total number of such configurations grows *sub-exponentially* $\sim 2^{\sqrt{N}}$, which should be contrasted with the dimer covering problem, where this number is known³¹ to be exponentially large. Based on this distinction, one may speculate that if our plaquette picture is valid, there are not enough different plaquette configurations for the paramagnetic phase to become a spin liquid (i.e., a *resonant plaquette state*). This statement, certainly, needs a separate investigation.

Finally, we emphasize that a main goal of this work is to investigate the fundamental symmetries of the phases exhibited by the J_1 - J_2 model. Although the energies presented for the 2×2 and 4×4 plaquette cases are different from those, obtained by more sophisticated numerical methods, they can be systematically improved by considering correlated trial wavefunctions or by using

more complex methods, which build upon the results reported here. However, we expect that symmetry-wise our conclusions will remain unchanged. One of such methods suited for computing the phase diagram of the model (1), which received significantly less attention, amounts to applying the Wilson renormalization group procedure³² and the density matrix renormalization group (DMRG) method⁸. Application of the latter faces serious difficulties in 2D (see Ref. 33 for a related discussion) and requires a mapping of the 2D system onto a chain, which introduces a certain bias to the final results⁸. While formulation of a practical and efficient DMRG approach to 2D systems is yet to be developed, we note that our results may provide a useful and rational initial input for such an algorithm.

VI. CONCLUSION

In summary, we analysed the phase diagram of the 2D J_1 - J_2 model on a square lattice, focusing on the symmetries of various phases.

We showed that in this model the hierarchical language²² is defined by identifying the *plaquette as a relevant degree of freedom*. Using an unbiased and manifestly symmetry-conserving mean-field approach we compared it with several other possible candidates: dimer and cross degrees of freedom, as well as different ways to cover a 2D lattice with plaquettes. Our results indicate that the plaquette covering, which preserves the lattice rotational symmetry has the best energy and it is the only one to give the correct phase diagram of the model, while other possibilities fail to reproduce all quantum phase transition points.

Consistent with the previous work on the subject, we found the quantum paramagnetic phase in the interval $0.42 \leq J_2/J_1 \leq 0.66$. Main controversies revolve around the nature of this intermediate non-magnetic phase and of the quantum critical point separating it from the Néel-ordered state. We found that the paramagnetic phase is a *plaquette crystal*, preserving both lattice and spin rotational symmetries. Consequently, the Ginzburg-Landau-Wilson paradigm of phase transitions is perfectly applicable in this case. Indeed, there is a group-subgroup relation between symmetries of the Néel and non-magnetic phases, which are thus separated by a second-order phase transition. On the contrary, such relation does not exist between the plaquette crystal and columnar antiferromagnetic phases, so the corresponding transition is of the first order. Our plaquette crystal is quite different from the usually proposed dimerized (bond-ordered) phases in this non-magnetic region.

We also proposed a way to include fluctuations around the HF ground state and showed that properties of the collective excitation spectrum are consistent with the overall picture of spontaneously broken symmetries. In particular, it was demonstrated that the quantum paramagnetic state is characterized by a finite gap in the excita-

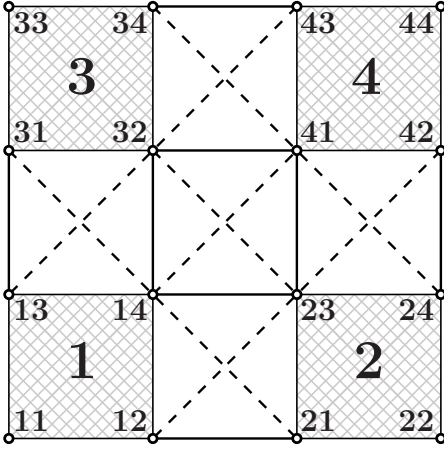


FIG. 13: The 4×4 superplaquette degree of freedom. Each spin carries two indices: a 2×2 plaquette number and a coordinate within this plaquette.

tion spectrum, which vanishes in the Néel and columnar phases, producing a doubly degenerate Goldstone mode.

Although currently there exists no known material whose ground state realizes the paramagnetic phase of the J_1 - J_2 model, in the future momentum-resolved measurements, such as neutron diffraction methods, can be used to identify the plaquette crystal phase of the type proposed here. Its experimental signature will be the unbroken four-fold lattice rotational symmetry on both sides of the second-order phase transition at the critical point J_2^c .

We acknowledge fruitful discussions with C. Eсеbbag and E. Fradkin. This work was supported in part by the

Spanish MEC under grant No. FIS2006-12783-C03-01.

VII. APPENDIX A: SUPERPLAQUETTE DEGREE OF FREEDOM

Here we present details of the HF calculation which uses the 4×4 superplaquette, shown in Fig. 13, as an elementary degree of freedom. It turns out that the full angular momentum basis is inconvenient, thus we use the 2×2 plaquette product states in order to perform the mean-field calculations. Each spin is characterized by two indices: the plaquette number $i = 1, \dots, 4$ and an index $n = 1 \dots 4$, which specifies a vertex in the plaquette. The singlet sector of the superplaquette Hilbert space is spanned by the states:

$$|A\rangle = \prod_{i=1}^4 |a_i\rangle,$$

where prime indicates the constraint $\sum_{i=1}^4 M_i = 0$. Using these states, we can write down matrix elements like

$$\langle a'_1 \dots a'_4 | \mathbf{S}_{in} \mathbf{S}_{jn'} | a_1 \dots a_4 \rangle$$

in the compact form:

$$\langle A' | \mathbf{S}_{in} \mathbf{S}_{jn'} | A \rangle = (\sigma_{nn'})_{a_i a_j}^{a'_i a'_j} \prod_{l \neq i, j} \delta_{a'_l a_l} \quad (17)$$

with the symmetric matrices $(\sigma_{nm})_{a_i a_j}^{a'_i a'_j} = (\sigma_{mn})_{a_j a_i}^{a'_j a'_i} = (\sigma_{nm})_{a'_i a'_j}^{a_i a_j}$ defined as:

$$\begin{aligned} (\sigma_{nn'})_{a_i a_j}^{a'_i a'_j} &= \sum_{K, M} (-1)^{L_i + L'_j + K} \langle L'_i M'_i L'_j M'_j | L'_i L'_j K M \rangle \langle L_i M_i L_j M_j | L_i L_j K M \rangle \times \\ &\quad \times \begin{Bmatrix} L'_i & L'_j & K \\ L_j & L_i & 1 \end{Bmatrix} \langle \lambda'_i || S_n || \lambda_i \rangle \langle \lambda'_j || S'_n || \lambda_j \rangle, \end{aligned}$$

The Hamiltonian of a single superplaquette consists of two parts: a diagonal one, involving only 2×2 plaquette contributions and a non-diagonal part, which accounts for the plaquette interactions. The former is written down straightforwardly as a matrix:

$$(H_d)_{A'A} = \prod_i \delta_{a'_i a_i} \sum_i \epsilon_{a_i}, \quad (18)$$

where ϵ_a is the plaquette self-energy, Eq. (4). The non-diagonal part has the operator form:

$$\begin{aligned} H_{\text{nd}} &= J_1 [(\mathbf{S}_{14} + \mathbf{S}_{41})(\mathbf{S}_{23} + \mathbf{S}_{32}) + \mathbf{S}_{12} \mathbf{S}_{21} + \mathbf{S}_{13} \mathbf{S}_{31} + \mathbf{S}_{34} \mathbf{S}_{43} + \mathbf{S}_{24} \mathbf{S}_{42}] + \\ &\quad + J_2 [\mathbf{S}_{12} \mathbf{S}_{23} + \mathbf{S}_{14} \mathbf{S}_{21} + \mathbf{S}_{23} \mathbf{S}_{42} + \mathbf{S}_{41} \mathbf{S}_{24} + \mathbf{S}_{34} \mathbf{S}_{41} + \mathbf{S}_{32} \mathbf{S}_{43} + \\ &\quad + \mathbf{S}_{31} \mathbf{S}_{14} + \mathbf{S}_{13} \mathbf{S}_{32} + \mathbf{S}_{14} \mathbf{S}_{41} + \mathbf{S}_{32} \mathbf{S}_{23}]. \end{aligned} \quad (19)$$

Let us now proceed with interaction terms in the J_1 - J_2 Hamiltonian (1). Each superplaquette has 4 nearest and 4 next-nearest neighbors. Within each neighboring superplaquette we enumerate 2×2 plaquettes by the indices 5,

6, 7, 8, so that $1 \rightarrow 5$, $2 \rightarrow 6$, $3 \rightarrow 7$ and $4 \rightarrow 8$. Enumeration of vertices within a plaquette stays the same. In this manner we have the symmetrized nearest neighbor

$$\begin{aligned}
H_1 = & \frac{J_1}{4} [\mathcal{S}_{11}(\mathcal{S}_{73} + \mathcal{S}_{62}) + \mathcal{S}_{12}\mathcal{S}_{74} + \mathcal{S}_{13}\mathcal{S}_{64} + \mathcal{S}_{31}\mathcal{S}_{82} + \mathcal{S}_{34}\mathcal{S}_{52} + \mathcal{S}_{33}(\mathcal{S}_{84} + \mathcal{S}_{51}) + \\
& + \mathcal{S}_{21}\mathcal{S}_{83} + \mathcal{S}_{24}\mathcal{S}_{53} + \mathcal{S}_{22}(\mathcal{S}_{84} + \mathcal{S}_{51}) + \mathcal{S}_{43}\mathcal{S}_{61} + \mathcal{S}_{42}\mathcal{S}_{71} + \mathcal{S}_{44}(\mathcal{S}_{73} + \mathcal{S}_{62})] + \\
& + \frac{J_2}{4} [\mathcal{S}_{11}(\mathcal{S}_{74} + \mathcal{S}_{64}) + \mathcal{S}_{12}(\mathcal{S}_{73} + \mathcal{S}_{83}) + \mathcal{S}_{13}(\mathcal{S}_{62} + \mathcal{S}_{82}) + \mathcal{S}_{21}(\mathcal{S}_{74} + \mathcal{S}_{84}) \\
& + \mathcal{S}_{22}(\mathcal{S}_{53} + \mathcal{S}_{83}) + \mathcal{S}_{24}(\mathcal{S}_{51} + \mathcal{S}_{71}) + \mathcal{S}_{31}(\mathcal{S}_{84} + \mathcal{S}_{64}) + \mathcal{S}_{33}(\mathcal{S}_{82} + \mathcal{S}_{52}) + \\
& + \mathcal{S}_{34}(\mathcal{S}_{51} + \mathcal{S}_{61}) + \mathcal{S}_{42}(\mathcal{S}_{73} + \mathcal{S}_{53}) + \mathcal{S}_{43}(\mathcal{S}_{62} + \mathcal{S}_{52}) + \mathcal{S}_{44}(\mathcal{S}_{71} + \mathcal{S}_{61})],
\end{aligned} \tag{20}$$

and next-nearest neighbor

$$H_2 = \frac{J_2}{4} [\mathcal{S}_{11}\mathcal{S}_{84} + \mathcal{S}_{22}\mathcal{S}_{73} + \mathcal{S}_{33}\mathcal{S}_{62} + \mathcal{S}_{44}\mathcal{S}_{51}] \tag{21}$$

superplaquette interactions. Using Eq. (17), one can easily construct matrix elements of the operators (19)-(21), which are required to obtain the HF equation of the type (11).

Having computed the single-superplaquette ground state wavefunction $R_A^0 = R_{a_1 a_2 a_3 a_4}^0$, we can use it to determine the spin polarizations:

$$\begin{aligned}
\langle \text{HF} | S_{1n}^z | \text{HF} \rangle &= (S_n^z)_{a'_1 a_1} R_{a'_1 a_2 a_3 a_4}^0 R_{a_1 a_2 a_3 a_4}^0; \\
&\vdots \\
\langle \text{HF} | S_{4n}^z | \text{HF} \rangle &= (S_n^z)_{a'_4 a_4} R_{a_1 a_2 a_3 a'_4}^0 R_{a_1 a_2 a_3 a_4}^0,
\end{aligned}$$

where $(S_n^z)_{a'_a}$ is given by Eq. (13).

VIII. APPENDIX B: FLUCTUATION CORRECTIONS – SUPERFLUID MEAN-FIELD

In this Appendix we extend the analysis of Sec. III by considering fluctuations around the HF ground state. While not unique, a natural way to achieve this goal is to perform a superfluid-type mean-field approximation. As a result one can obtain the collective spectrum and corrections to the GSE and magnetization. Of primary interest is, of course, the energy gap in the excitation spectrum.

The structure of the superfluid mean-field is similar to the Fetter-Bogoliubov approach to inhomogeneous Bose liquids³⁴. Although we present results only for the 2×2 plaquette degree of freedom, it can equally be applied to the 4×4 superplaquette case.

Let us return to the original Hamiltonian (8) and explicitly separate out the condensate mode in the operators γ_{ia} :

$$\gamma_{ia} = g_a + \beta_{ia}. \tag{22}$$

The condensation will occur in a certain superposition of the single-plaquette states. The real-valued multiplet

g_a plays the role of a condensate wavefunction (CWF)³⁴. Here it is chosen to be spatially homogeneous, but inhomogeneous phases can also be included. The CWF is normalized to the condensate fraction:

$$\sum_a g_a^2 = n_0.$$

The non-condensate bosonic operators β_{ia} describe fluctuation corrections to the HF solution. If they are neglected, we naturally return to the results of Sec. III. It is important to observe, however, that the HF ground state corresponds to the Bose condensation on *each* lattice site, not only in the $\mathbf{k} = 0$ mode.

The superfluid mean-field approximation amounts to enforcing the Schwinger boson constraint on average:

$$n_0 + \frac{1}{N_\square} \sum_{i,a} \langle \beta_{ia}^\dagger \beta_{ia} \rangle = 1, \tag{23}$$

neglecting fluctuations in the condensate channel, and retaining only terms quadratic in β in the Hamiltonian (8):

$$\begin{aligned}
H = & N_\square \left[\frac{1}{2} \left(\mu n_0 + \sum_a \epsilon_a g_a^2 \right) - \mu n_0 \right] + \\
& + \sum_{i,a} (\epsilon_a - \mu) \beta_{ia}^\dagger \beta_{ia} + 4 \sum_{i,\sigma} (H_{\text{int}}^\sigma)_{a_1 a_2}^{a'_1 a'_2} g_{a'_1} g_{a'_2} \beta_{i a'_1}^\dagger \beta_{i a_1} + \\
& + \sum_{\sigma, \langle ij \rangle_\sigma} (H_{\text{int}}^\sigma)_{a_1 a_2}^{a'_1 a'_2} [g_{a'_1} g_{a'_2} (\beta_{i a_1}^\dagger \beta_{j a_2}^\dagger + \beta_{i a_1} \beta_{j a_2}) + \\
& + 2g_{a_1} g_{a_2} \beta_{i a_1}^\dagger \beta_{j a_2}],
\end{aligned} \tag{24}$$

where we abbreviated $\langle ij \rangle_\sigma = (\langle ij \rangle, \langle \langle ij \rangle \rangle)$ and matrix elements of H_{int}^σ are given by Eq. (5).

The CWF g_a is determined by the Gross-Pitaevskii equation, similar to the HF equation (11):

$$\left\{ \epsilon_a \delta_{aa'} + 4 \sum_\sigma (H_{\text{int}}^\sigma)_{a' a_2}^{a a_1} g_{a_1} g_{a_2} \right\} g_{a'} = \mu g_a, \tag{25}$$

which defines the chemical potential μ and guarantees the disappearance of linear terms in β from the Hamiltonian of Eq. (24). It is clear that $g_a(n_0 = 1) = R_a^0$ and $\mu(n_0 =$

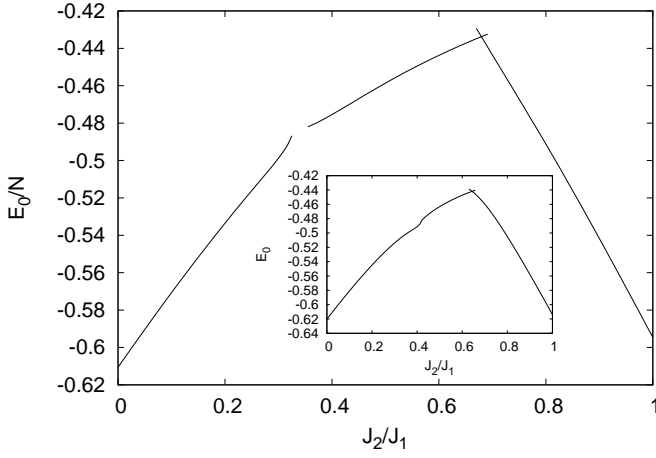


FIG. 14: Ground state energy for the self-consistent solution (main panel) and after the first iteration (inset). The critical point J_2^{c1} becomes a λ -point. The absence of points in the main panel around J_2^{c1} is due to bad convergence in the simulation.

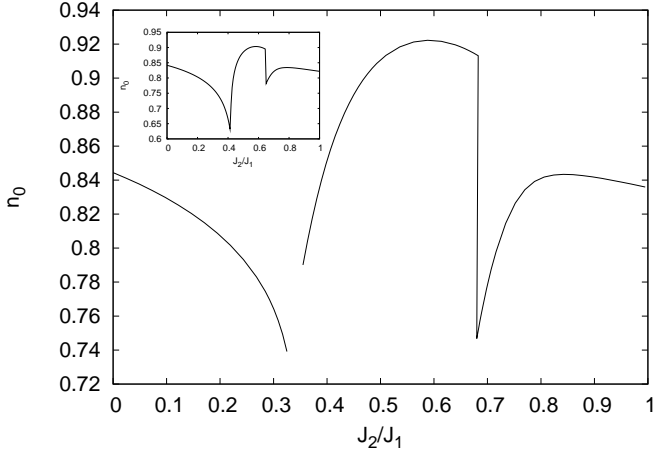


FIG. 15: Condensate fraction for the self-consistent solution (main panel) and after the first iteration (inset). Notice the shift of quantum phase transition points $J_2^{c1,2}$.

$1) = \varepsilon_0$. In other words, Eq. (25) reproduces the results of Sec. III, if n_0 is forced to be unity. Naturally, the first line in Eq. (24) coincides in this limit (up to the chemical potential) with the expression (12) for E_0 . Quadratic terms in Eq. (24) represent fluctuation corrections to the HF results and constitute the focus of our analysis below.

The next step is to transform the quadratic part (H_2) of the Hamiltonian in Eq. (24) into momentum space:

$$\begin{aligned}
 H_2 = & \sum_{\mathbf{k}, a} (\varepsilon_a - \mu) \beta_{\mathbf{k}a}^\dagger \beta_{\mathbf{k}a} + \sum_{\mathbf{k}, \sigma} (H_{\text{int}}^\sigma)_{a_1 a_2}^{a_1' a_2'} \{ \Theta_{\mathbf{k}}^\sigma [g_{a_1'} g_{a_2'} \times \\
 & \times (\beta_{\mathbf{k}a_1'}^\dagger \beta_{-\mathbf{k}a_2'}^\dagger + \beta_{\mathbf{k}a_1} \beta_{\mathbf{k}a_2}) + 2g_{a_1} g_{a_2'} \beta_{\mathbf{k}a_1'}^\dagger \beta_{\mathbf{k}a_2'}] + \\
 & + 4g_{a_2'} g_{a_2} \beta_{\mathbf{k}a_1'}^\dagger \beta_{\mathbf{k}a_1} \}, \quad (26)
 \end{aligned}$$

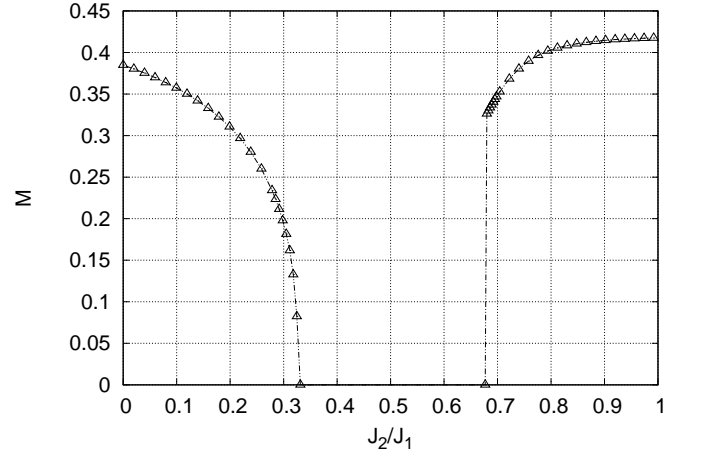


FIG. 16: Self-consistently computed staggered magnetization, M_{stag} , for $J_2 \leq J_2^{c1}$ and columnar magnetization along the x -direction, $M_{\text{col}}(x)$, for $J_2 \geq J_2^{c2}$.

where $\Theta_{\mathbf{k}}^\sigma = (\cos k_x + \cos k_y, 2 \cos k_x \cos k_y)$ and \mathbf{k} is defined within the plaquette Brillouin zone (i.e., there are N_{\square} \mathbf{k} -states). This Hamiltonian can be diagonalized by the Bogoliubov's transformation:

$$\begin{aligned}
 \alpha_{\mathbf{k}\nu} &= \sum_a (u_{\mathbf{k}a}^\nu \beta_{\mathbf{k}a} - v_{\mathbf{k}a}^\nu \beta_{-\mathbf{k}a}^\dagger); \\
 \alpha_{-\mathbf{k}\nu}^\dagger &= \sum_a (-v_{\mathbf{k}a}^\nu \beta_{\mathbf{k}a} + u_{\mathbf{k}a}^\nu \beta_{-\mathbf{k}a}^\dagger), \quad (27)
 \end{aligned}$$

to a new set of bosonic operators $\alpha_{\mathbf{k}\nu}$, which represent quasiparticle excitations and annihilate the new ground state: $\alpha_{\mathbf{k}\nu} |\Psi_0\rangle = 0$. Of course, only positive quasiparticle energies, labelled by ν , have physical meaning, however, in order to obtain closure relations for the wavefunction ($u_{\mathbf{k}a}^\nu, v_{\mathbf{k}a}^\nu$) (which is, obviously, even in \mathbf{k}), we need to include zero-energy eigenvectors as well³⁵. This completeness relation has the form, valid for *all* wavevectors:

$$\begin{aligned}
 \sum_{\nu} (u_{\mathbf{k}a}^\nu u_{\mathbf{k}b}^\nu - v_{\mathbf{k}a}^\nu v_{\mathbf{k}b}^\nu) &= \delta_{ab}; \\
 \sum_{\nu} (u_{\mathbf{k}a}^\nu v_{\mathbf{k}b}^\nu - v_{\mathbf{k}a}^\nu u_{\mathbf{k}b}^\nu) &= 0. \quad (28)
 \end{aligned}$$

The amplitudes $u_a^\nu(\mathbf{k})$ and $v_a^\nu(\mathbf{k})$ are determined from Bogoliubov's equations:

$$\begin{aligned}
 U_{ab}^N(\mathbf{k}) u_{\mathbf{k}b}^\nu + U_{ab}^A(\mathbf{k}) v_{\mathbf{k}b}^\nu &= \omega_\nu(\mathbf{k}) u_{\mathbf{k}a}^\nu; \\
 U_{ab}^A(\mathbf{k}) u_{\mathbf{k}b}^\nu + U_{ab}^N(\mathbf{k}) v_{\mathbf{k}b}^\nu &= -\omega_\nu(\mathbf{k}) v_{\mathbf{k}a}^\nu, \quad (29)
 \end{aligned}$$

where we have introduced symmetric matrices:

$$\begin{aligned}
 U_{ab}^N(\mathbf{k}) &= \frac{1}{2} (\varepsilon_a - \mu) \delta_{ab} + \sum_{\sigma} (H_{\text{int}}^\sigma)_{a_2 b}^{a a_1} \Theta_{\mathbf{k}}^\sigma g_{a_1} g_{a_2} + \\
 & + 2 \sum_{\sigma} (H_{\text{int}}^\sigma)_{b a_2}^{a a_1} g_{a_1} g_{a_2}; \quad (30) \\
 U_{ab}^A(\mathbf{k}) &= \sum_{\sigma} (H_{\text{int}}^\sigma)_{ab}^{a_1 a_2} \Theta_{\mathbf{k}}^\sigma g_{a_1} g_{a_2}.
 \end{aligned}$$

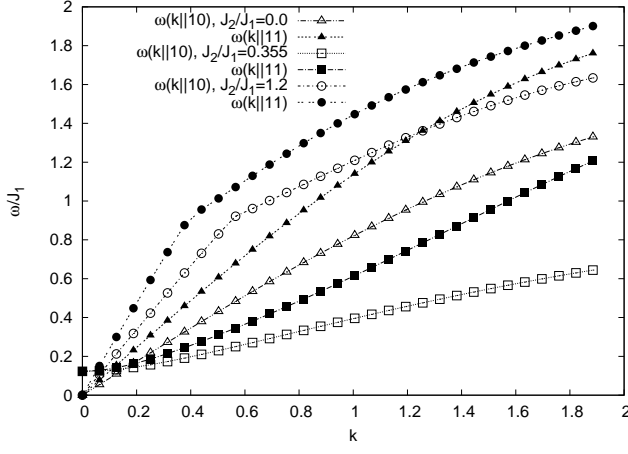


FIG. 17: The lowest excitation branch $\omega_1(\mathbf{k})$ along the [10] and [11] directions for three values of J_2/J_1 chosen in different phases.

It follows from Eq. (29) that at each \mathbf{k} the quasiparticle amplitudes obey the orthogonality conditions:

$$\begin{aligned} \sum_a (u_{\mathbf{k}a}^\nu u_{\mathbf{k}a}^{\nu'} - v_{\mathbf{k}a}^\nu v_{\mathbf{k}a}^{\nu'}) &= \delta_{\nu\nu'}; \\ \sum_a (u_{\mathbf{k}a}^\nu v_{\mathbf{k}a}^{\nu'} - v_{\mathbf{k}a}^\nu u_{\mathbf{k}a}^{\nu'}) &= 0. \end{aligned} \quad (31)$$

For any value of \mathbf{k} Bogoliubov's equations (29) always have at least two zero eigenvalues, which correspond to the zero-norm eigenvector $u = -v = g$. This means that our case differs fundamentally from the canonical superfluid Bose gas: instead of having a macroscopic number of particle in one particular energy state, we obtain a macroscopic number (equal to N_\square) of condensation modes, each containing less than one boson.

The quasiparticle energy equals $2\omega_\nu(\mathbf{k})$ and the GSE, condensate fraction and spin polarization are expressed in terms of $u_{\mathbf{k}a}^\nu$ and $v_{\mathbf{k}a}^\nu$ as:

$$\begin{aligned} \frac{E_0}{N} &= \frac{1}{8} \left(\mu n_0 + \sum_a \epsilon_a g_a^2 \right) + \frac{1}{4} \mu (1 - n_0) - \\ &\quad - \frac{2}{N} \sum'_{\mathbf{k}, \nu, a} \omega_\nu(\mathbf{k}) (v_{\mathbf{k}a}^\nu)^2; \\ n_0 &= 1 - \frac{1}{N_\square} \sum'_{\mathbf{k}, \nu, a} (v_{\mathbf{k}a}^\nu)^2; \\ \langle S_{in}^z \rangle &= (S_n^z)_{a'a} \left[g_a' g_a + \frac{1}{N_\square} \sum'_{\mathbf{k}, \nu} v_{\mathbf{k}a'}^\nu v_{\mathbf{k}a}^\nu \right]. \end{aligned} \quad (32)$$

In this expression \mathbf{k} -summations are extended over the plaquette Brillouin zone and ν -summations over positive eigenvalues of Eq. (29), as indicated by the primes.

The condensate fraction n_0 should, in principle, be determined self-consistently. The approximation is reasonable if $n_0 \sim 1$. However, close to the phase transition points this is not true, since fluctuations are very large

in their vicinity. But deeply in each phase the approximation works reasonably well, because n_0 turns out to be of the order of 0.9. Results of the numerical solution of Eqs. (25), (29) and (32) for the symmetric covering of the lattice with 2×2 plaquettes are shown in Figs. 14-17. The system size is 100×100 plaquettes and periodic boundary conditions are assumed. Figures' main panels correspond to the self-consistent solution and their insets give results after the first iteration, which is equivalent to solving the time-dependent Gross-Pitaevskii equation³⁵. Due to bad convergence close to the transition points (see, for instance, Fig. 14) the values of J_2^{c1} and J_2^{c2} were determined by extrapolation: $J_2^{c1} \approx 0.33J_1$ and $J_2^{c2} \approx 0.65J_1$. The large shift of J_2^{c1} compared to the HF value is due to fluctuations in the β -channel, which renders this point to be a λ -point, reduces the nominal value of the magnetization in the Néel phase down to $M(J_2 = 0) \approx 0.37$ (Fig. 16), and causes a great suppression of the condensate, as shown in Fig. 15.

However, the most interesting quantity to observe is the gap in the excitation spectrum. Due to the homogeneity of the plaquette lattice, it occurs at $\mathbf{k} = 0$ and is shown in Fig. 11.

Technically, one may show that its very existence reflects the nature of the ground state in the paramagnetic phase. Indeed, introducing linear combinations of the amplitudes u and v : $\varphi = u + v$ and $\chi = u - v$, Bogoliubov's Eq. (29) can be rewritten in the form:

$$(U^N + U^A)(U^N - U^A)\chi = \omega^2 \chi.$$

In the non-magnetic phase the condensation occurs in the lowest plaquette state $|1100\rangle$: $g_a = \sqrt{n_0} \delta_{a,1100}$ and the chemical potential coincides with its energy: $\mu = \epsilon_{1100}$. Moreover, the matrix $\sum_\sigma (H_{\text{int}}^\sigma)_{b,1100}^{a,1100}$ vanishes. Writing down the remaining matrices in (30) at $\mathbf{k} = 0$, it is easy to see that there exists only one vector χ , which is annihilated by $(U^N - U^A)$. Outside the intermediate region this simple situation is not valid and there exist three eigenvectors χ , which correspond to $\omega^2 = 0$. One of them is the condensate mode and should be discarded. The other two give doubly degenerate Goldstone modes in the Néel and columnar phases. Here the self-consistent field, determined by g_a , breaks the spin-rotational symmetry of the original Hamiltonian. However, since the CWF g_a belongs to the $M = 0$ subspace, the generator S_z remains an integral of motion. Thus, there should be two Goldstone modes associated with rotations around the x and y axes³⁵.

Our approximation correctly describes the excitation spectrum only at small \mathbf{k} . However, this is more than enough to observe that the collective modes are of the spin-wave type in the Néel and columnar phases, while in the paramagnetic phase the excitation band is parabolic. These conclusions are summarized in Fig. 17, where we show the lowest branch $\omega_1(\mathbf{k})$ along two directions $\mathbf{k} \parallel [10]$ and $\mathbf{k} \parallel [11]$ for three values of J_2/J_1 , chosen in different phases.

-
- ¹ S. Sachdev, *Quantum Phase Transitions* (Cambridge University Press, Cambridge, 1999).
- ² G. Misguich and C. Lhuillier in *Frustrated Spin Systems*, edited by H. T. Diep (World Scientific, Singapore, 2004).
- ³ P. Carretta *et al.*, Phys. Rev. Lett. **88**, 047601 (2002); A. Bombardi *et al.*, *ibid.* **93**, 027202 (2004).
- ⁴ P. Carretta *et al.*, Phys. Rev. **B66**, 094420 (2002).
- ⁵ R. Nath *et al.*, arXiv:0803.3535v1 [cond-mat.str-el].
- ⁶ L. Capriotti and S. Sorella, Phys. Rev. Lett. **84**, 3173 (2000).
- ⁷ L. Capriotti *et al.*, Phys. Rev. Lett. **87**, 097201 (2001).
- ⁸ M. S. L. du Croo de Jongh *et al.*, Phys. Rev. **B62**, 14844 (2000).
- ⁹ R. Darradi *et al.*, cond-mat/0806.3825v1.
- ¹⁰ R. R. P. Singh *et al.*, Phys. Rev. **B60**, 7278 (1999).
- ¹¹ K. Takano *et al.*, Phys. Rev. Lett. **91**, 197202 (2003).
- ¹² V. Kotov *et al.*, Phys. Rev. **B60**, 14613 (1999).
- ¹³ V. Lante and A. Parola, Phys. Rev. **B73**, 094427 (2006).
- ¹⁴ N. Read and S. Sachdev, Phys. Rev. Lett. **66**, 1773 (1991).
- ¹⁵ T. Senthil *et al.*, Phys. Rev. **B70**, 144407 (2004).
- ¹⁶ L. D. Landau, E. M. Lifshitz and L. P. Pitaevskii, *Statistical Physics*, parts. 1 and 2 (Butterworth-Heinemann, New-York, 1999); K. G. Wilson and J. Kogut, Phys. Rep. **12**, 75 (1974).
- ¹⁷ E. Manousakis, Rev. Mod. Phys. **63**, 1 (1991).
- ¹⁸ That the translational symmetry is broken in the Néel phase is easy to see, if one *assumes* broken spin $SU(2)$ symmetry. Then, due to the principle of weakening of correlations, the staggered correlation function satisfies:
- $$\lim_{|i-j| \rightarrow \infty} (-1)^{i-j} \langle S_i^z S_j^z \rangle = (-1)^{i-j} \langle S_i^z \rangle \langle S_j^z \rangle,$$
- which can be constant only if $\langle S_i^z \rangle$ depends on i .
- ¹⁹ J. Sirker *et al.*, Phys. Rev. **B73**, 184420 (2006).
- ²⁰ A. W. Sandvik, Phys. Rev. Lett. **98**, 227202 (2007).
- ²¹ C. D. Batista and S. A. Trugman, Phys. Rev. Lett. **93**, 217202 (2004).
- ²² G. Ortiz and C. D. Batista, Phys. Rev. **B67**, 134301 (2003), in *Condensed Matter Theories*, vol. 18, M. de Llano *et al.* (ed.), Nova Science Publishers, 2003.
- ²³ M. van den Bossche *et al.*, Eur. Phys. J. **B17**, 367 (2000).
- ²⁴ E. Altman and A. Auerbach, Phys. Rev. **B65**, 104508 (2002).
- ²⁵ A. R. Edmonds, *Angular Momentum in Quantum Mechanics* (Princeton University Press, Princeton, 1957).
- ²⁶ A. Auerbach, *Interacting Electrons and Quantum Magnetism* (Springer-Verlag, New York, 1994).
- ²⁷ C. K. Majumdar and D. K. Ghosh, J. Math. Phys. **10**, 1388 (1969).
- ²⁸ K. Okamoto and K. Nomura, Phys. Lett. **A169**, 433 (1992).
- ²⁹ E. H. Lieb, T. D. Schultz and D. C. Mattis, Ann. Phys. **16**, 407 (1961).
- ³⁰ M. B. Hastings, Phys. Rev. **B69**, 104431 (2004).
- ³¹ M. E. Fisher, Phys. Rev. **124**, 1664 (1961).
- ³² F. Kruger and S. Scheidl, Europhys. Lett. **74**, 896 (2006).
- ³³ S. R. White, Phys. Rev. Lett. **77**, 3633 (1996).
- ³⁴ A. L. Fetter, Ann. Phys. **70**, 67 (1972).
- ³⁵ J. P. Blaizot and G. Ripka, *Quantum theory of finite systems* (The MIT Press, Cambridge, 1986).